Article

The New Semiconductor Cs4Cu3Bi9S17

Jing Zhao, Saiful M. Islam, Gangjian Tan, Shiqiang Hao, Chris Wolverton, R. K. Li, and Mercouri G. Kanatzidis

Chem. Mater., **Just Accepted Manuscript** • DOI: 10.1021/acs.chemmater.6b05298 • Publication Date (Web): 10 Jan 2017

The New Semiconductor $Cs_4Cu_3Bi_9S_{17}$

Jing Zhao, [1, 2] Saiful M. Islam, [2] Gangjian Tan, [2] Shiqiang Hao, [3] Chris Wolverton, [3] R. K. Li, [1] Mercouri G. Kanatzidis [2, *]

[1]Beijing Center for Crystal Research and Development, Technical Institute of Physics and Chemistry, Chinese Academy of Sciences, Beijing, 100190, P. R. China
[2]Department of Chemistry, Northwestern University, Evanston, Illinois 60208, United States
[3]Department of Materials Science and Engineering, Northwestern University, Evanston, Illinois 60208, United States

ABSTRACT

New quaternary chalcogenide $Cs_4Cu_3Bi_9S_{17}$ has been synthesized by solid state reaction in a vacuum sealed silica tube. $Cs_4Cu_3Bi_9S_{17}$ adopts the monoclinic space group $P2_1/m$, with a = 20.006(4) Å, b = 4.0556(8) Å, c = 22.279(5) Å and β = 96.921°. The crystal structure of $Cs_4Cu_3Bi_9S_{17}$ features a unique three-dimensional framework consisting of interconnected Bi_2Te_3- and CdI_2-type fragments forming three different sized tunnels running parallel to the b-axis. The tunnels are filled with different numbers (1, 2, 4) of Cs atoms. $Cs_4Cu_3Bi_9S_{17}$ is stable in air at room temperature and differential thermal analysis showed that it decomposes at elevated temperature. $Cs_4Cu_3Bi_9S_{17}$ is a semiconductor with a direct optical band gap of 0.9 eV which is in agreement with density functional theory calculations. Electrical conductivity and Seebeck coefficient measurements show n-type semiconductor behavior. The electrical conductivity is 10^{-4} S/cm at 300 K and increases to 0.9 S/cm at 773 K. $Cs_4Cu_3Bi_9S_{17}$ possesses a very low thermal conductivity of 0.71 $Wm^{-1}K^{-1}$ at room temperature which decreases linearly with rising temperature to 0.46 $Wm^{-1}K^{-1}$ at 773 K. The low thermal conductivity shows $Cs_4Cu_3Bi_9S_{17}$ is promise as a new thermoelectric material with appropriate doping.

To whom correspondence should be addressed: m-kanatzidis@northwestern.edu

INTRODUCTION

Bismuth chalcogenides exhibit immense compositional and structural diversity.[1] The stereochemical activity of $6s^2$ lone pair makes Bi^{3+} extremely flexible in its bonding with coordination numbers varying from 3 to 9 and leads to several coordination geometries. If the lone pair is stereochemically suppressed it can form normal octahedral geometry with six almost equidistant Bi-Q bonds (Q = S, Se, Te).[1, 2] More commonly, Bi^{3+} cations are found in severely distorted octahedral geometries with coordination environments that resemble capped octahedra,[3] capped trigonal prisms,[2] or a trigonal bipyramid with long and short Bi···Q bonds.[4] Often in complex structures bismuth participates in mixed site occupation with similarly sized atoms, e.g. Pb, Sn, lanthanide, alkali or alkaline earth metal atoms.[5-7] Generally, Bi polyhedra share edges or faces to form various building blocks that derive from the NaCl-, Bi_2Te_3-, CdI_2-, and Sb_2Se_3-type structures.[1, 8] These blocks come in different shapes and sizes and are usually connected either directly to each other or through other metal atoms. These characteristics lead to the wide diversity of novel structures.[9]

Alkali metals in general reside between layers or in tunnels created by covalent bismuth chalcogenide frameworks, and because they are ionically interacting with the framework they tend to "rattle".[10, 11] Occasionally however when the alkali atoms are similar in size to the main group metals in the covalent framework mixed occupancy can occur.[12, 13] The rattling motion of the cations in the tunnels can decrease the thermal conductivity, while the ordered framework serves to propagate the charge carriers. This effect is related to the so-called phonon-glass/electron crystal (PGEC) mechanism proposed by Slack;[14] the typical PGEC system includes clathrates,

skutterudites and chalcogenides. Structural complexity in compounds containing heavy elements also favors low lattice thermal conductivity. For example, β-$K_2Bi_8Se_{13}$ includes two different interconnected types of Bi/Se blocks, K ions positional and compositionally disordered with Bi ions over the same crystallographic sites, and with loosely bound K atoms in tunnels,[5] which shows promising thermoelectric properties by virtue of its very low thermal conductivity (~1.3 W/m·K).[15, 16] $CsBi_4Te_6$ has a layered structure with slabs of $[Bi_4Te_6]^-$ alternating with layers of Cs^+ ions.[17] $CsBi_4Te_6$ contains both formally Bi^{3+} and Bi^{2+} centers the latter forming Bi-Bi bonds. The lattice thermal conductivity value parallel to the layers is ~1.1 W/m·K at room temperature.[17, 18]

Clearly, developing Bi-chalcogenide chemistry is important and further inspired by their high structural complexity as well as diversity of the physical properties.[6, 8] Herein, we investigated the quaternary bismuth-systems using copper as the fourth element. The choice of chalcophilic Cu derives from the expectation that its unique coordination preferences, mainly tetrahedral, will result in unique structure types in framework containing also Bi. Previous investigations of the systems A/Cu/Bi/Q (A = K, Rb, Cs, Q = S and Se) led to four structure types in the compounds: ABi_2CuS_4 (A = K, Cs)[19, 20], $A_3Bi_5Cu_2S_{10}$ (A = K, Rb, Cs)[19, 20], $KBiCu_2S_3$[21] and $RbBi_{2.66}CuSe_5$[20]. These materials exhibit considerable structural complexity. ABi_2CuS_4 (A = K, Cs), $A_3Bi_5Cu_2S_{10}$ (A = K, Rb, Cs) and $RbBi_{2.66}CuSe_5$ have a three-dimensional structure while $KBiCu_2S_3$ has a layered structure with K^+ cation reside between the layers.

In this work, we describe the new chalcogenide $Cs_4Cu_3Bi_9S_{17}$ and its physical

properties. It reveals an unprecedented three-dimensional framework with cesium filling in three different sized tunnels. $Cs_4Cu_3Bi_9S_{17}$ has a band gap of 0.9 eV which according to density functional theory calculations is direct. $Cs_4Cu_3Bi_9S_{17}$ is an n-type semiconductor with a conductivity of 10^{-4} S/cm at 300 K and 0.9 S/cm at 773 K. $Cs_4Cu_3Bi_9S_{17}$ exhibits extremely low thermal conductivity with 0.46 $Wm^{-1}K^{-1}$ at 773 K and the mechanism of the low thermal conductivity is discussed.

EXPERIMENTAL SECTION

Reagents. All chemicals were used as obtained: copper metal (99.9%, Strem Chemicals, Inc., Newburyport, MA), bismuth metal (99.9%, Strem Chemicals, Inc., Newburyport, MA), sulfur pellets (99.99%, Sigma Aldrich, St. Louis, MO). Cs_2S were synthesized by reacting stoichiometric amounts of the elements in liquid ammonia as described elsewhere.[22]

Synthesis and Crystal Growth. Stoichiometric amounts of Cs_2S, Cu, Bi, and S were combined together (~2.3 g total mass) in a 9 mm fused silica tube in a dry, nitrogen-filled glovebox. The tubes were evacuated to $\sim 10^{-4}$ mbar and flame sealed. The sealed tube was put into a 13 mm tube and sealed with a vacuum of $\sim 10^{-4}$ bar. The tubes were then placed into a programmable furnace and heated to 300 ^{o}C in 6 h, held at this temperature for 6 h, then heated to 1000 ^{o}C in 12 h and held for 18 h before cooling down to room temperature (RT) in 24 h. This procedure yielded $Cs_4Cu_3Bi_9S_{17}$ with a yield of almost 100%.

Powder X-ray Diffraction. The purity of the sample was examined by powder X-ray diffraction (PXRD) using a Rigaku Miniflex powder X-ray diffractometer with

Ni-filtered Cu Kα radiation operating at 30 kV and 15 mA. The experiment was conducted with a scan width of 0.02^{o} and a rate of 10^{o}/min. The simulated PXRD pattern was obtained by using the CIF of the refined structure in the Visualizer software package of the program FINDIT.

Single Crystal X-ray Diffraction. A STOE IPDS II single crystal diffractometer operating at 50 kV and 40 mA was used to conduct X-ray diffraction measurement with Mo Kα radiation (λ = 0.71073 Å). A single crystal with dimensions of 0.0652 × 0.0056 × 0.0045 mm^3 was adhered to the tip of a glass fiber with glue. Data collection was performed using X-Area software,[23] integration was carried out in X-RED, and a numerical absorption correction was applied with X-SHAPE, both X-RED and X-SHAPE[23] are programs provided by STOE. The crystal structures were solved via direct methods and refined with the SHELXTL program package.[24] The crystal data and structure refinement results are shown in Table 1 and selected bond lengths in Table 2.

Scanning Electron Microscopy. Quantitative microprobe analyses and crystal imaging of the compound were performed with Hitachi S-3400 scanning electron microscope equipped with a PGT energy-dispersive X-ray analyzer. Data were acquired using an accelerating voltage of 25 kV, 70 mA probe current, and 60 s acquisition time. The compositions reported here are the results of averaging a large number of independent measurements from a given sample.

Differential Thermal Analysis. Differential thermal analysis (DTA) was performed with a computer-controlled Shimadzu DTA-50 thermal analyzer. The

ground single crystals with total mass about 50 mg were sealed in a silica ampoule under a vacuum. A silica ampoule containing alumina of equal mass was sealed and placed on the reference side of the detector. The samples were heated to 800 °C at 10 °C/min followed by cooling at 10 °C/min to room temperature and finally this cycle was repeated. The DTA residual sample was examined with powder X-ray diffraction after the experiment.

Infrared and Ultraviolet-visible Spectroscopy. Optical diffuse reflectance measurement was carried out on finely ground samples at room temperature. The spectrum was recorded, in the infrared region 300-2500 nm, with the use of UV-3600 Shimadzu UV-3600 PC double-beam, double-monochromator spectrophotometer. The measurement of diffuse reflectivity can be used to obtain values for the band gap that agrees rather well with the values obtained by transmission measurements from single crystals of the same material. Absorption (α/S) data was calculated from the reflectance data using Kubelka−Munk equation: $\alpha/S = (1-R)^2/2R$, where R is reflectance, α is the absorption coefficient, and S is the scattering coefficient.[3] The absorption edge was estimated by linearly fitting the absorbance of the converted data.

Density Functional Theory (DFT) Calculations. The total energies and relaxed geometries were calculated by DFT within the generalized gradient approximation of Perdew−Burke−Ernzerhof the exchange correlation functional with Projector Augmented Wave potentials.[25] We use periodic boundary conditions and a plane wave basis set as implemented in the Vienna ab initio simulation package.[26] The total

energies were numerically converged to approximately 3 meV/cation with spin-orbit coupling using a basis set energy cutoff of 500 eV and dense k-meshes corresponding to 4000 per reciprocal atom k-points in the Brillouin zone. Our theoretically relaxed low-temperature $Cs_4Cu_3Bi_9S_{17}$ lattice constants are a = 20.23 Å, b = 4.08 Å, and c = 22.51 Å, which are in good agreement with the experimentally measured one of a = 19.91 Å, b = 4.04 Å, and c = 22.25 Å.

Spark Plasma Sintering. Homogeneously ground powders were loaded into 10 mm diameter graphite dies for densification using spark plasma sintering (SPS) method (SPS-211LX, Fuji Electronic Industrial Co. Ltd.). The SPS condition was 763 K for 5 min under an axial pressure of 30 MPa. Then round shape pellet with 10 mm diameter and 7 mm thickness was finally obtained, and its relative mass density is about 89%. Figure S1 shows the PXRD of the ground powder of post SPS sample.

Electrical Properties. The SPS pellet was cut into bars with dimensions ~2.3 × 2.2 × 7.39 mm^3 for measurement of electrical conductivity using an Ulvac Riko ZEM-3 instrument under a low-pressure helium atmosphere from room temperature to 773 K. The uncertainties of electrical conductivity measurements are 10%.[27] In this study the electrical conductivity was measured perpendicular to the sintering pressure direction.

Thermal Conductivity. The obtained SPS processed pellets was cut and polished into a cube with dimensions of ~6.0 × 6.0 × 1.2 mm^3 for thermal diffusivity measurements. The sample was coated with a thin layer of graphite to minimize errors from the emissivity of the material and the thermal diffusion direction is perpendicular to the sintering pressure direction. The thermal conductivity was

calculated from $\kappa = DC_pd$, where the thermal diffusivity coefficient (D) was measured by using the laser flash diffusivity method in a Netzsch LFA457 in the range of 300-773 K, the specific heat capacity (C_p) was calculated by Dulong-Petit law $C_p = 3R/\overline{M}$ where R is the gas constant 8.314 $J \cdot mol^{-1}K^{-1}$ and $\overline{M}$ is the average molar mass (95.4 for $Cs_4Cu_3Bi_9S_{17}$), and the density (d) was calculated to be 5.17 g/cm^3 by using the dimensions and mass of the sample and which is 89% of the theoretical density. The thermal diffusivity data were analyzed using a Cowan model with pulse correction and the uncertainty of the thermal conductivity is within 16%.[27]

RESULTS AND DISCUSSION

Syntheses and Thermal Behavior. Single phase of $Cs_4Cu_3Bi_9S_{17}$ was synthesized by heating a stoichiometric mixture of Cs_2S, Cu, Bi and S in sealed silica tube at 1000 ^oC. Microcrystalline $Cs_4Cu_3Bi_9S_{17}$ was obtained with a cooling rate of 42 $^oC/h$ while slower cooling rate ~10 $^oC/h$ produced single crystallites up to ~0.1 mm edge length which are suitable for single crystal diffraction. As judged by X-ray powder diffraction the obtained sample is pure, Figure 1. This compound is black and it is stable in air, water and organic solvents such as ethanol, acetone and DMF. Energy-dispersive X-ray spectroscopy (EDS) performed as semiquantitative elemental analysis of Cs, Cu, Bi and S, gave the composition as "$Cs_4Cu_{2.9}Bi_{9.2}S_{17.3}$", which is in agreement with the composition obtained from the refinement of the crystal structure. (Figure S2).

Differential thermal analysis (DTA) was used to understand the thermal behavior of $Cs_4Cu_3Bi_9S_{17}$. The compound was heated to 800 °C and cooled down to room

temperature at a rate of 10 °C/min. Two consecutive heating-cooling cycles in the DTA revealed an endothermic peak at 576 °C and two exothermic peaks at 568 °C and 510 °C (Figure 2). This suggests that $Cs_4Cu_3Bi_9S_{17}$ melts incongruently. In the second cycle the endothermic peak at 576 °C can be clearly seen suggesting that in the first cycle the decomposition is not completed. Also, a broad endothermic peak around 490 °C seen in the second heating cycle corresponds to the melting of the decomposed compounds. In the second cooling section the crystallization exothermic peak at 568 °C disappeared indicating nearly complete decomposition of $Cs_4Cu_3Bi_9S_{17}$. PXRD of the DTA products showed that the compound totally decomposed to an unknown phase after heating to 800 °C for two cycles (Figure S3). Although it melts incongruently, by using the heating profile mentioned above sample almost >99% pure was obtained. This may due to the decomposed phases appear on the way up in temperature. When the system melts fully at ~1000 ^{o}C the reaction homogenizes again. Then on cooling the crystallization occurs to give the correct compound perhaps along with some minor phases. During the slow cooling of the crystallized solids solid state equilibria likely drive the reaction to the $Cs_4Cu_3Bi_9S_{17}$ as the main product.

Crystal Structure. $Cs_4Cu_3Bi_9S_{17}$ crystallizes in a unique structure in the monoclinic space group $P2_1/m$. Its asymmetric unit contains nine bismuth, three copper, four cesium and seventeen crystallographically unique sulfur atoms (Figure 3a). All atoms occupy a general Wyckoff position 2e. The crystal structure of $Cs_4Cu_3Bi_9S_{17}$ is a new type and is formed by the covalent bismuth-sulfur and

copper-sulfur interactions while cesium atoms exhibit ionic interactions with neighboring sulfur atoms (Figure 3b). The anionic framework consists of Bi_2Te_3- and CdI_2- type structural blocks which are interconnected by three distorted CuS_4 and three distorted BiS_6 octahedral units (Figure 4). The bismuth atoms of the face-sharing octahedra share their edges with $Cu(3)S_4$ and $Cu(1)S_4$ tetrahedra respectively.

The Bi···Bi non-bonding interatomic distances range from 3.621(2) to 4.3234(9) Å. The shortest are between Bi6 and Bi9 a face sharing octahedra (Bi6-Bi9 = 3.621(2) Å). The framework features three different parallel tunnels which are occupied by the cesium cations. Two of these distinct types of tunnels are shared with the neighboring unit cells while the third one, which is the smallest, remains exclusively in the unit cell of $Cs_4Cu_3Bi_9S_{17}$.

The coordination geometries of the bismuth atoms are shown in Figure 5. All are coordinated by six sulfur atoms with Bi-S distances ranging from 2.646(8) to 3.263(13) Å and an average bond distance of 2.866 Å. These bond lengths clearly reflect the strong distortions in the BiS_6 octahedra. The Bi-S distances are similar to previously reported ones, e.g. $CsPbBi_3S_6$[28], $Pb_2La_xBi_{8-x}S_{14}$[7] and $Cs_3Cu_2Bi_5S_{10}$[19]. Selected bond distances and angles in the structure of $Cs_4Cu_3Bi_9S_{17}$ are given in Table 2. This strongly distorted octahedral coordination environment arises from the stereochemical activity of the $6s^2$ lone pair of bismuth as seen previously for example in $KBi_{6.33}S_{10}$[29] and $K_2Bi_8S_{13}$[30].

There are three different crystallographic Cu sites bonding to sulfur atoms in a form

of distorted tetrahedra (Figure 6). The CuS_4 tetrahedra of the Cu1 and Cu2 exhibit nearly four equal Cu-S bonds ranging from 2.344(9) to 2.487(9) Å. The Cu3 atom is coordinated to sulfur with three short ~2.319(5) Å and one long 2.789(8) Å bonds to form a strongly distorted tetrahedron. There are four crystallographically different kinds of cesium atoms residing in the three different types of tunnels (Figure 3b). Cs3 resides in the narrowest tunnels while Cs1 appears in pairs in the wider tunnels. The Cs2 and Cs4 reside in the widest tunnels. The sulfur atoms form three-, five- and six-fold coordination polyhedra.

As in ABi_2CuS_4 (A = K, Cs)[19, 20], $A_3Bi_5Cu_2S_{10}$ (A = K, Rb, Cs)[19, 20] and $KBiCu_2S_3$[21], Cu in $Cs_4Cu_3Bi_9S_{17}$ adopts the +1 oxidation state. Among these sulfides, octahedrally coordinated Bi and tetrahedrally coordinated Cu are seen for ABi_2CuS_4 (A = K, Cs) and $A_3Bi_5Cu_2S_{10}$ (A = K, Rb, Cs), however, $KBiCu_2S_3$ exhibits both triangular and tetrahedral coordination Cu and three coordinated Bi (Figure 7). By comparison to these, $Cs_4Cu_3Bi_9S_{17}$ exhibits much more intricate crystal structure with 9 different coordination environments of Bi and three different Cu atoms giving a larger three-dimensional framework with three different sized tunnels.

The Band Gap and DFT Calculations. The solid state electronic absorption spectra measured from a polycrystalline sample of $Cs_4Cu_3Bi_9S_{17}$ showed a very steep absorption edge at ~0.9 eV indicating a semiconductor, Figure 8. DFT electronic band structure calculations indicate the presence of a direct band gap of 0.6 eV. The under-estimation of the calculated band gap is well known for GGA (Figure 9a).[31] The conduction and valence band extrema are found at Γ (0.0, 0.0, 0.0).

Figure 9b shows the projected density of states (DOS) to analyze the electronic contribution of band structure. Clearly, the valence band maximum (VBM) is mainly composed of Cu 3d and S 3p states, while the conduction band minimum (CBM) is made predominantly from Bi 6p states. The effective masses m* were calculated by fitting the E-k bands around the CBM for the different directions with the definition:

$$m^* = \hbar^2 \left(\frac{\partial^2 E}{\partial k^2} \right)^{-1}$$

where ħ is the reduced Planck constant. The calculated effective mass at first CBM along the Γ-X, Γ-Y, and Γ-Z direction are respectively $m^*_{\Gamma Y} = 0.78\ m_0$, $m^*_{\Gamma X} = 1.02\ m_0$, $m^*_{\Gamma Z} = 0.12\ m_0$. On the basis of the above three effective mass components by using the formula $m = (g^2 m^*_{\Gamma Y} m^*_{\Gamma X} m^*_{\Gamma Z})^{\frac{1}{3}}$ (g is degeneracy which is 5 for $Cs_4Cu_3Bi_9S_{17}$) it is easy to get the density of state (DOS) effective mass 1.33 m_0 for $Cs_4Cu_3Bi_9S_{17}$. The DOS effective mass is very close to the DOS effective mass of SnSe 1.20 m_0, which includes the multiband effects.[32] The relative large effective mass directly induce the relative large Seebeck coefficient about -460 μV/K (at dilute concentration of 1×10^{17} cm^{-3} at 300 K), which is comparable to the SnSe at undoped case about 500 μV/K at 300 K.[36]

Thermal Conductivity and Electrical Conductivity. Samples of $Cs_4Cu_3Bi_9S_{17}$ exhibit a large Seebeck coefficient of -445 V/K at ~50 °C which shows it is an n-type conductor. The thermal diffusivity was measured perpendicular to the sintering pressure (Figure S4). Figure 10a shows that the thermal conductivity of $Cs_4Cu_3Bi_9S_{17}$ is ~0.71 $Wm^{-1}K^{-1}$ at 300 K and decreases almost linearly with increasing temperature, to a very low value of ~0.46 $Wm^{-1}K^{-1}$ at 773 K. The $Cs_4Cu_3Bi_9S_{17}$ SPSed sample is 89% of the calculated density, which may contain porous and thus lead to underestimate of

thermal conductivity. Here, we use the modified formulation of the effective medium theory to calculate the intrinsic lattice thermal conductivity.[33] A simplified expression for the lattice thermal conductivity of porous media is shown as follow:

$$\kappa_{eff} = \kappa_h \frac{2-2\Phi}{2+2\Phi}$$

in the equation κ_{eff} is the effective thermal conductivity which can be measured, κ_h is the intrinsic thermal conductivity of the host, and Φ is the porosity and for the SPSed $Cs_4Cu_3Bi_9S_{17}$ sample we used it is 0.11. Therefore, the intrinsic thermal conductivity of the host material (κ_h) is calculated and was shown in Figure S5. From the figure we can see the host thermal conductivity of $Cs_4Cu_3Bi_9S_{17}$ is ~ 0.9 $Wm^{-1}K^{-1}$, which is still intrinsically low. The thermal conductivity of $Cs_4Cu_3Bi_9S_{17}$ at high temperature is comparable to that of glasses and nanocrystalline materials. For example, KSb_5S_8 glass has a thermal conductivity of 0.50 $Wm^{-1}K^{-1}$ at 300 K;[34] nanocrystalline bulk BiSbTe with thermal conductivity of 1.15 $Wm^{-1}K^{-1}$ at 300 K[35] and PbTe alloy nanostructured with SrTe and Na with thermal conductivity of 0.9 $Wm^{-1}K^{-1}$ at 900 K[36].

The high temperature thermal conductivity values of $Cs_4Cu_3Bi_9S_{17}$ are comparable to those of the recently explored SnSe compound with highly anharmonic chemical bonding.[37-39] The mechanism behind the intrinsically low thermal conductivity of $Cs_4Cu_3Bi_9S_{17}$ is related to the larger unit cell of the complex crystal structure and perhaps to the cesium cations in the tunnels that may be engaged in "rattler" activity. The complex structure of $Cs_4Cu_3Bi_9S_{17}$ leads to increase of the lattice period thus providing short mean path length by presenting a longer more "tortuous" path way for

the heat carrying phonons. The rattler atoms have been invoked as phonon scattering centers in many compounds including $Cs_2Hg_6S_7$[10], $Ba_8Au_{16}P_{30}$[40] and $CsAg_5Te_3$[41].

The temperature dependent electrical conductivity of polycrystalline SPSed sample of $Cs_4Cu_3Bi_9S_{17}$ is given in Figure 10b. The electrical conductivity is thermally activated and ranges between 10^{-4} and 0.9 S/cm from 300 to 773 K. The conductivity at 300 K is comparable to that of $Rb_3Bi_5Cu_2S_{10}$ and two orders lower than KBi_2CuS_4.[19] The low electrical conductivity and high Seebeck coefficient indicate a low number of charge carriers consistent with the fact that the $Cs_4Cu_3Bi_9S_{17}$ samples are undoped.

CONCLUDING REMARKS

The new compound $Cs_4Cu_3Bi_9S_{17}$ adopts a unique structure type with a tunneled three-dimensional framework. There are three different sized tunnels in $Cs_4Cu_3Bi_9S_{17}$ running parallel to the *b*-axis in which cesium atoms reside. $Cs_4Cu_3Bi_9S_{17}$ is a semiconductor with an optical band gap of 0.9 eV and DFT calculations show it is a direct semiconductor. $Cs_4Cu_3Bi_9S_{17}$ shows a Seebeck coefficient of -445 V/K at room temperature. The electrical conductivity of $Cs_4Cu_3Bi_9S_{17}$ is ~10^{-4} S/cm at 300 K and increases with temperature with the highest of 0.9 S/cm at 773 K. Due to the complicated tunneled structure and perhaps to the "rattling" alkali metal reside in the tunnels the material features a very low thermal conductivity of 0.71 $Wm^{-1}K^{-1}$ at 300 K and ~0.46 $Wm^{-1}K^{-1}$ at 773 K.

ASSOCIATED CONTENT

Supporting Information

X-ray crystallographic data of $Cs_4Cu_3Bi_9S_{17}$ in CIF format. Tables of atomic

coordinates and displacement parameters of $Cs_4Cu_3Bi_9S_{17}$; figures of the PXRD of the SPSed sample; SEM image and Energy-dispersive X-ray spectroscopy spectrum; PXRD before and after DTA and thermal diffusivity are given in supporting information. This material is available free of charge via the Internet at http://pubs.acs.org.

Author information

Corresponding Author

*E-mail: m-kanatzidis@northwestern.edu

Notes

The authors declare no competing financial interest.

ACKNOWLEDGMENTS

This work was supported by the National Science Foundation Grant DMR-1410169 (synthesis). This work was supported by the Department of Energy, Office of Science, Basic Energy Sciences under grant DE-SC0014520 (thermal transport, electronic structure calculations. SMI is supported by MRSEC program (NSF DMR-1121262). This work made use of the EPIC facility (NUANCE Center-Northwestern University), which has received support under the State of Illinois, Northwestern University, and the National Science Foundation with grants DMR-1121262 through the MRSEC program at the Materials Research Center, and EEC-0118025/003 through The Nanoscale Science and Engineering Center.

REFERENCES:

1. Iordanidis, L.; Bilc, D.; Mahanti, S. D.; Kanatzidis, M. G. Impressive structural diversity and polymorphism in the modular compounds ABi_3Q_5 (A = Rb, Cs; Q = S, Se, Te). *J. Am. Chem. Soc.* **2003,** *125*, 13741-13752.

2. Iordanidis, L.; Brazis, P. W.; Kyratsi, T.; Ireland, J.; Lane, M.; Kannewurf, C. R.; Chen, W.; Dyck, J. S.; Uher, C.; Ghelani, N. A.; Hogan, T.; Kanatzidis, M. G. $A_2Bi_8Se_{13}$ (A = Rb, Cs), $CsBi_{3.67}Se_6$, and $BaBi_2Se_4$: New ternary semiconducting bismuth selenides. *Chem. Mater.* **2001,** *13*, 622-633.

3. McCarthy, T. J.; Ngeyi, S. P.; Liao, J. H.; DeGroot, D. C.; Hogan, T.; Kannewurf, C. R.; Kanatzidis, M. G. Molten salt synthesis and properties of three new solid-state ternary bismuth chalcogenides, .beta.-$CsBiS_2$, .gamma.-$CsBiS_2$, and $K_2Bi_8Se_{13}$. *Chem. Mater.* **1993,** *5*, 331-340.

4. Iordanidis, L.; Schindler, J. L.; Kannewurf, C. R.; Kanatzidis, M. G. $ALn_{1\pm x}Bi_{4\pm x}S_8$ (A = K, Rb; Ln = La, Ce, Pr, Nd): New semiconducting quaternary bismuth sulfides. *J. Solid State Chem.* **1999,** *143*, 151-162.

5. Hoang, K.; Tomic, A.; Mahanti, S. D.; Kyratsi, T.; Chung, D. Y.; Tessmer, S. H.; Kanatzidis, M. G. Role of K/Bi disorder in the electronic structure of beta-$K_2Bi_8Se_{13}$. *Phys. Rev. B* **2009,** *80*, 125112.

6. Kim, J. H.; Chung, D. Y.; Kanatzidis, M. G. A new chalcogenide homologous series $A_2[M_{5+n}Se_{9+n}]$ (A = Rb, Cs; M = Bi, Ag, Cd). *Chem. Commun.* **2006**, 1628-1630.

7. Iordanidis, L.; Kanatzidis, M. G. Novel quaternary lanthanum bismuth sulfides $Pb_2La_xBi_{8-x}S_{14}$, $Sr_2La_xBi_{8-x}S_{14}$, and $Cs_2La_xBi_{10-x}S_{16}$ with complex structures. *Inorg. Chem.* **2001,** *40*, 1878-1887.

8. Kanatzidis, M. G. Structural evolution and phase homologies for "design" and prediction of solid-state compounds. *Acc. Chem. Res.* **2005,** *38*, 359-368.

9. Mrotzek, A.; Kanatzidis, M. G. "Design" in solid-state chemistry based on phase homologies. The concept of structural evolution and the new megaseries $A_m[M_{1+l}Se_{2+l}]_{2m}[M_{2l+n}Se_{2+3l+n}]$. *Acc. Chem. Res.* **2003,** *36*, 111-119.

10. Li, H.; Peters, J. A.; Liu, Z.; Sebastian, M.; Malliakas, C. D.; Androulakis, J.; Zhao, L.; Chung, I.; Nguyen, S. L.; Johnsen, S. Crystal growth and characterization of the X-ray and *γ*-ray detector material $Cs_2Hg_6S_7$. *Cryst. Growth Des.* **2012,** *12*, 3250-3256.

11. Nolas, G. S.; Vanderveer, D. G.; Wilkinson, A. P.; Cohn, J. L. Temperature dependent structural and transport properties of the type II clathrates $A_8Na_{16}E_{136}$(A = Cs or Rb and E = Ge or Si). *J. Appl. Phys.* **2002,** *91*, 8970-8973.

12. Gabrel'yan, B.; Lavrentiev, A.; Nikiforov, I. Y.; Sobolev, V. Electronic energy structure of $MBiS_2$ (M = Li, Na, K) calculated with allowance for the difference between the MS and Bi-S bond lengths. *J. Struct. Chem.* **2008,** *49*, 788-794.

13. Chung, D.-Y.; Choi, K.-S.; Iordanidis, L.; Schindler, J. L.; Brazis, P. W.; Kannewurf, C. R.; Chen, B.; Hu, S.; Uher, C.; Kanatzidis, M. G. High thermopower and low thermal conductivity in semiconducting ternary K−Bi−Se compounds. synthesis and properties of *β*-$K_2Bi_8Se_{13}$ and $K_{2.5}Bi_{8.5}Se_{14}$ and their Sb analogues. *Chem. Mater.* **1997,** *9*, 3060-3071.

14. Rowe, D. M. *CRC handbook of thermoelectrics*; CRC press: New York, 1995.

15. Kyratsi, T.; Dyck, J. S.; Chen, W.; Chung, D. Y.; Uher, C.; Paraskevopoulos, K. M.; Kanatzidis, M. G. Highly anisotropic crystal growth and thermoelectric properties of $K_2Bi_{8-x}Sb_xSe_{13}$ solid solutions: Band gap anomaly at low *x*. *J. Appl. Phys.* **2002,** *92*, 965-975.

16. Pei, Y.; Chang, C.; Wang, Z.; Yin, M.; Wu, M.; Tan, G.; Wu, H.; Chen, Y.; Zheng, L.; Gong, S.; Zhu, T.; Zhao, X.; Huang, L.; He, J.; Kanatzidis, M. G.; Zhao, L.-D. Multiple converged conduction bands in

$K_2Bi_8Se_{13}$: A promising thermoelectric material with extremely low thermal conductivity. *J. Am. Chem. Soc.* **2016,** *138*, 16364-16371.

17. Chung, D. Y.; Hogan, T. P.; Rocci-Lane, M.; Brazis, P.; Ireland, J. R.; Kannewurf, C. R.; Bastea, M.; Uher, C.; Kanatzidis, M. G. A new thermoelectric material: $CsBi_4Te_6$. *J. Am. Chem. Soc.* **2004,** *126*, 6414-6428.

18. Chung, D. Y.; Hogan, T.; Brazis, P.; Rocci-Lane, M.; Kannewurf, C.; Bastea, M.; Uher, C.; Kanatzidis, M. G. $CsBi_4Te_6$: A high-performance thermoelectric material for low-temperature applications. *Science* **2000,** *287*, 1024-1027.

19. Yang, Y. T.; Brazis, P.; Kannewurf, C. R.; Ibers, J. A. Structures and conductivities of the quaternary A/Bi/Cu/S phases KBi_2CuS_4 and $A_3Bi_5Cu_2S_{10}$ (A = Rb, Cs). *J. Solid State Chem.* **2000,** *155*, 243-249.

20. Huang, F. Q.; Mitchell, K.; Ibers, J. A. Syntheses and structures of the quaternary alkali-metal bismuth coinage-metal chalcogenides $K_3Bi_5Cu_2S_{10}$, $CsBi_2CuS_4$, $RbBi_{2.66}CuSe_5$, and $CsBiAg_2S_3$. *J. Alloys Compd.* **2001,** *325*, 84-90.

21. Zhang, G. H.; Zhang, B. W.; Chen, H. J.; Zhang, X.; Zheng, C.; Lin, J. H.; Huang, F. Q. Synthesis and characterization of a novel quaternary chalcogenide $KBiCu_2S_3$. *J. Alloys Compd.* **2014,** *591*, 6-10.

22. Hanko, J. A.; Sayettat, J.; Jobic, S.; Brec, R.; Kanatzidis, M. G. $A_2CuP_3S_9$ (A = K, Rb), $Cs_2Cu_2P_2S_6$, and $K_3CuP_2S_7$: New phases from the dissolution of copper in molten polythiophosphate fluxes. *Chem. Mater.* **1998,** *10*, 3040-3049.

23. X-AREA, X.-R., and X-SHAPE； Cie & Stoe: Darmstadt,. X-AREA, X-RED, and X-SHAPE. Germany, 1998.

24. Sheldrick, G. A short history of SHELX. *Acta Crystallogr., Sect. A: Found. Adv.* **2008,** *64*, 112-122.

25. Perdew, J. P.; Burke, K.; Ernzerhof, M. Generalized gradient approximation made simple. *Phys. Rev. Lett.* **1996,** *77*, 3865.

26. Kresse, G.; Furthmüller, J. Efficient iterative schemes for ab initio total-energy calculations using a plane-wave basis set. *Phys. Rev. B* **1996,** *54*, 11169.

27. Borup, K. A.; de Boor, J.; Wang, H.; Drymiotis, F.; Gascoin, F.; Shi, X.; Chen, L. D.; Fedorov, M. I.; Muller, E.; Iversena, B. B.; Snyder, G. J. Measuring thermoelectric transport properties of materials. *Energy Environ. Sci.* **2015,** *8*, 423-435.

28. Chung, D. Y.; Iordanidis, L.; Rangan, K. K.; Brazis, P. W.; Kannewurf, C. R.; Kanatzidis, M. G. First quaternary A-Pb-Bi-Q (A = K, Rb, Cs; Q = S, Se) compounds: Synthesis, structure, and properties of alpha- and beta-$CsPbBi_3Se_6$, $APbBi_3Se_6$, (A = K, Rb), and $APbBi_3S_6$ (A = Rb, Cs). *Chem. Mater.* **1999,** *11*, 1352-1362.

29. Kanatzidis, M. G.; McCarthy, T. J.; Tanzer, T. A.; Chen, L.-H.; Iordanidis, L.; Hogan, T.; Kannewurf, C. R.; Uher, C.; Chen, B. Synthesis and thermoelectric properties of the new ternary bismuth sulfides $KBi_{6.33}S_{10}$ and $K_2Bi_8S_{13}$. *Chem. Mater.* **1996,** *8*, 1465-1474.

30. Iordanidis, L.; Brazis, P. W.; Kannewurf, C. R.; Kanatzidis, M. G. Synthesis and thermoelectric properties of $Cs_2Bi_{7.33}Se_{12}$, $A_2Bi_8Se_{13}$ (A = Rb, Cs), $Ba_{4-x}Bi_{6+2/3x}Se_{13}$, and $Ba_{3\pm x}Pb_{3\pm x}Bi_6Se_{15}$. *MRS Proceedings* **1998,** *545*.

31. Bilc, D. I.; Mahanti, S. D.; Kyratsi, T.; Chung, D. Y.; Kanatzidis, M. G.; Larson, P. Electronic structure of $K_2Bi_8Se_{13}$. *Phys. Rev. B* **2005,** *71*.

32. Zhao, L. D.; Tan, G. J.; Hao, S. Q.; He, J. Q.; Pei, Y. L.; Chi, H.; Wang, H.; Gong, S. K.; Xu, H. B.; Dravid, V. P.; Uher, C.; Snyder, G. J.; Wolverton, C.; Kanatzidis, M. G. Ultrahigh power factor and thermoelectric performance in hole-doped single-crystal SnSe. *Science* **2016,** *351*, 141-144.

33. Lee, H.; Vashaee, D.; Wang, D.; Dresselhaus, M. S.; Ren, Z.; Chen, G. Effects of nanoscale porosity on thermoelectric properties of SiGe. *J. Appl. Phys.* **2010,** *107*, 094308.

34. Wachter, J. B.; Chrissafis, K.; Petkov, V.; Malliakas, C. D.; Bilc, D.; Kyratsi, T.; Paraskevopoulos, K. M.; Mahanti, S. D.; Torbrügge, T.; Eckert, H.; Kanatzidis, M. G. Local structure and influence of bonding on the phase-change behavior of the chalcogenide compounds $K_{1-x}Rb_xSb_5S_8$. *J. Solid State Chem.* **2007,** *180*, 420-431.

35. Poudel, B.; Hao, Q.; Ma, Y.; Lan, Y.; Minnich, A.; Yu, B.; Yan, X.; Wang, D.; Muto, A.; Vashaee, D.; Chen, X.; Liu, J.; Dresselhaus, M. S.; Chen, G.; Ren, Z. High-thermoelectric performance of nanostructured bismuth antimony telluride bulk alloys. *Science* **2008,** *320*, 634-638.

36. Biswas, K.; He, J. Q.; Blum, I. D.; Wu, C. I.; Hogan, T. P.; Seidman, D. N.; Dravid, V. P.; Kanatzidis, M. G. High-performance bulk thermoelectrics with all-scale hierarchical architectures. *Nature* **2012,** *489*, 414-418.

37. Zhao, L. D.; Lo, S. H.; Zhang, Y. S.; Sun, H.; Tan, G. J.; Uher, C.; Wolverton, C.; Dravid, V. P.; Kanatzidis, M. G. Ultralow thermal conductivity and high thermoelectric figure of merit in SnSe crystals. *Nature* **2014,** *508*, 373-377.

38. Zhao, L. D.; Tan, G. J.; Hao, S. Q.; He, J. Q.; Pei, Y. L.; Chi, H.; Wang, H.; Gong, S. K.; Xu, H. B.; Dravid, V. P. Ultrahigh power factor and thermoelectric performance in hole-doped single-crystal SnSe. *Science* **2016,** *351*, 141-144.

39. Wei, T. R.; Tan, G. J.; Zhang, X. M.; Wu, C. F.; Li, J. F.; Dravid, V. P.; Snyder, G. J.; Kanatzidis, M. G. Distinct impact of alkali-ion doping on electrical transport properties of thermoelectric p-type polycrystalline SnSe. *J. Am. Chem. Soc.* **2016,** *138*, 8875-8882.

40. Fulmer, J.; Lebedev, O. I.; Roddatis, V. V.; Kaseman, D. C.; Sen, S.; Dolyniuk, J. A.; Lee, K.; Olenev, A. V.; Kovnir, K. Clathrate $Ba_8Au_{16}P_{30}$: The "Gold Standard" for lattice thermal conductivity. *J. Am. Chem. Soc.* **2013,** *135*, 12313-12323.

41. Lin, H.; Tan, G.; Shen, J. N.; Hao, S.; Wu, L. M.; Calta, N.; Malliakas, C.; Wang, S.; Uher, C.; Wolverton, C. Concerted rattling in $CsAg_5Te_3$ leading to ultralow thermal conductivity and high thermoelectric performance. *Angew. Chem., Int. Ed.* **2016,** *55*, 11431-11436.

Tables:

Table 1. Crystal data and structure refinement for $Cs_4Cu_3Bi_9S_{17}$ at 293(2) K.

Empirical formula	$Cs_4Cu_3Bi_9S_{17}$
Formula weight	3148.10
Temperature	293(2) K
Wavelength	0.71073 Å
Crystal system	monoclinic
Space group	$P2_1/m$
Unit cell dimensions	a = 20.006(4) Å, α = 90.00° b = 4.0556(8) Å, β = 96.92(3)° c = 22.279(5) Å, γ = 90.00°
Volume	1794.4(6) $Å^3$
Z	2
Density (calculated)	5.826 g/cm^3
Absorption coefficient	50.680 mm^{-1}
F(000)	2652
Crystal size	0.0652 × 0.0056 × 0.0045 mm^3
θ range for data collection	2.83 to 25.00°
Index ranges	-23<=h<=23, -4<=k<=4, -25<=l<=26
Reflections collected	10929
Independent reflections	3620 [R_{int} = 0.0876]
Completeness to θ = 25.00°	99.3%
Refinement method	Full-matrix least-squares on F^2
Data / restraints / parameters	3620 / 0 / 200
Goodness-of-fit	1.057
Final R indices [>2σ(I)]	R_{obs} = 0.0513, wR_{obs} = 0.0909
R indices [all data]	R_{all} = 0.0829, wR_{all} = 0.0988
Extinction coefficient	0.00014(2)
Largest diff. peak and hole	1.959 and -2.613 $e \cdot Å^{-3}$

$R = \Sigma||F_o|-|F_c|| / \Sigma|F_o|$, $wR = \{\Sigma[w(|F_o|^2 - |F_c|^2)^2] / \Sigma[w(|F_o|^4)]\}^{1/2}$ and calc $w=1/[\sigma^2(Fo^2)+(0.0383P)^2+0.0000P]$ where $P=(Fo^2+2Fc^2)/3$

Table 2. Bond lengths [Å] for $Cs_4Cu_3Bi_9S_{17}$ at 293(2) K with estimated standard deviations in parentheses.

Label	Distances	Label	Distances	Label	Distances
Bi(1)-S(9)#1	2.785(8)	Bi(4)-S(2)	2.874(6)	Bi(8)-S(6)	2.706(5)
Bi(1)-S(4)	2.827(7)	Bi(4)-S(4)#4	3.101(7)	Bi(8)-S(7)#3	3.024(6)
Bi(1)-S(9)#2	2.836(6)	Bi(5)-S(15)#2	2.699(5)	Bi(8)-S(7)#11	3.024(6)
Bi(1)-S(9)	2.836(6)	Bi(5)-S(15)	2.699(5)	Bi(8)-S(14)#3	3.038(7)
Bi(1)-S(1)	2.869(6)	Bi(5)-S(5)#6	2.768(7)	Bi(9)-S(12)	2.646(8)
Bi(1)-S(1)#2	2.869(6)	Bi(5)-S(17)#2	2.897(7)	Bi(9)-S(11)#2	2.715(4)
Bi(2)-S(1)	2.669(7)	Bi(5)-S(2)#6	3.000(6)	Bi(9)-S(11)	2.715(4)
Bi(2)-S(5)	2.724(5)	Bi(5)-S(2)#7	3.000(6)	Bi(9)-S(8)#2	3.005(6)
Bi(2)-S(5)#2	2.724(5)	Bi(6)-S(14)	2.754(5)	Bi(9)-S(8)	3.005(6)
Bi(2)-S(4)	2.928(6)	Bi(6)-S(14)#2	2.754(5)	Bi(9)-S(10)	3.263
Bi(2)-S(4)#4	2.928(6)	Bi(6)-S(7)	2.812(8)	Cu(1)-S(13)#2	2.344(9)
Bi(2)-S(2)	3.090(7)	Bi(6)-S(12)	2.883(7)	Cu(1)-S(12)#2	2.365(4)
Bi(3)-S(13)#2	2.693(5)	Bi(6)-S(8)#2	2.938(6)	Cu(1)-S(12)	2.365(4)
Bi(3)-S(13)	2.693(5)	Bi(6)-S(8)	2.938(6)	Cu(1)-S(14)#2	2.475(8)
Bi(3)-S(3)	2.716(7)	Bi(7)-S(16)	2.748(5)	Cu(2)-S(17)	2.386(5)
Bi(3)-S(9)#4	2.999(8)	Bi(7)-S(16)#2	2.748(5)	Cu(2)-S(17)#2	2.386(5)
Bi(3)-S(4)#5	3.041(6)	Bi(7)-S(16)#8	2.770(8)	Cu(2)-S(15)	2.407(8)
Bi(3)-S(4)#4	3.041(6)	Bi(7)-S(8)#9	2.835(8)	Cu(2)-S(6)	2.487(9)
Bi(4)-S(10)	2.589(7)	Bi(7)-S(7)#10	2.958(6)	Cu(3)-S(10)#9	2.319(5)
Bi(4)-S(3)#2	2.838(5)	Bi(7)-S(7)#9	2.958(6)	Cu(3)-S(10)#13	2.319(5)
Bi(4)-S(3)	2.838(5)	Bi(8)-S(17)#2	2.657(7)	Cu(3)-S(11)	2.331(9)
Bi(4)-S(2)#4	2.874(6)	Bi(8)-S(6)#2	2.706(5)	Cu(3)-S(3)#13	2.789(8)

Figures Captions :

Figure 1. The comparison of powder X-ray diffraction spectrum between synthesized $Cs_4Cu_3Bi_9S_{17}$ and the one simulated.

Figure 2. DTA curves of $Cs_4Cu_3Bi_9S_{17}$ reveal incongruent melting behavior.

Figure 3. The unit cell (a) and the tunneled structure (b) of $Cs_4Cu_3Bi_9S_{17}$.

Figure 4. The framework of $Cs_4Cu_3Bi_9S_{17}$ which contains Bi_2Te_3- and CdI_2-type blocks and three different sized tunnels in which cesium atoms reside; for clarity all Cs atoms were deleted. The frame on the right shows the details of the Bi- and Cu-polyhedra which connect the two different blocks together.

Figure 5. The coordination environments of Bi1 to Bi9.

Figure 6. The coordination environments of Cu1, Cu2 and Cu3.

Figure 7. The structure comparison between $Cs_4Cu_3Bi_9S_{17}$ (this paper) and other reported A-Cu-Bi-S (A = alkali metal) compounds.

Figure 8. UV-vis spectrum of $Cs_4Cu_3Bi_9S_{17}$ which has a direct band gap of 0.9 eV.

Figure 9. Band structure and corresponding Brillouin zone of $Cs_4Cu_3Bi_9S_{17}$; Total and partial density of states (DOS, eV/States) of $Cs_4Cu_3Bi_9S_{17}$.

Figure 10. Thermal conductivity (a) and electrical conductivity (b) values as a function of temperature for $Cs_4Cu_3Bi_9S_{17}$; the inset shows the SPSed sample and the bar and cube used for measurements.

TOC graphic

The new semiconductor $Cs_4Cu_3Bi_9S_{17}$ crystallizes in the monoclinic space group $P2_1/m$. $Cs_4Cu_3Bi_9S_{17}$ possesses a low thermal conductivity of 0.71 $Wm^{-1}K^{-1}$ at room temperature and ~0.46 $Wm^{-1}K^{-1}$ at 773 K. $Cs_4Cu_3Bi_9S_{17}$ has a direct band gap of 0.9 eV and it is an n-type semiconductor.

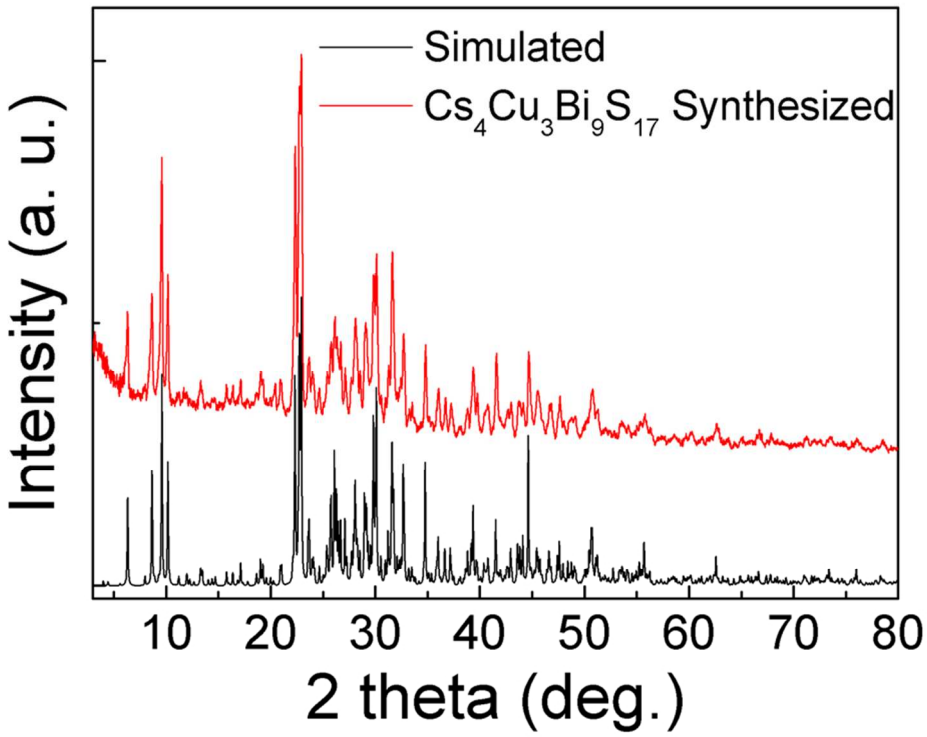

Figure 1. The comparison of powder X-ray diffraction spectrum between synthesized Cs4Cu3Bi9S17 and the one simulated.

84x66mm (300 x 300 DPI)

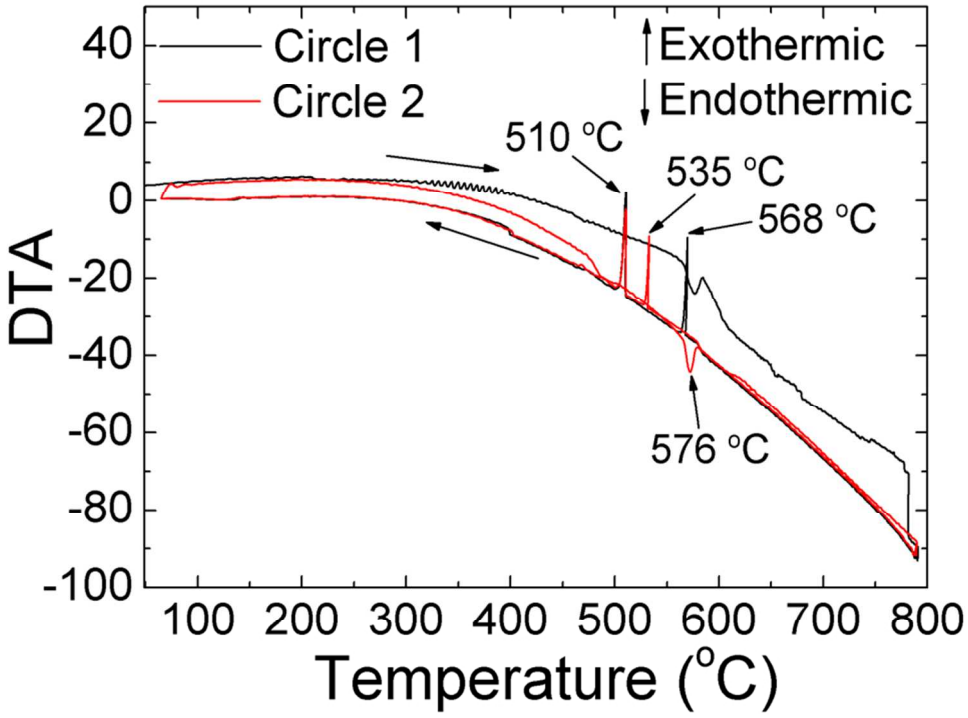

Figure 2. DTA curves of Cs4Cu3Bi9S17 reveal incongruent melting behavior.

84x63mm (300 x 300 DPI)

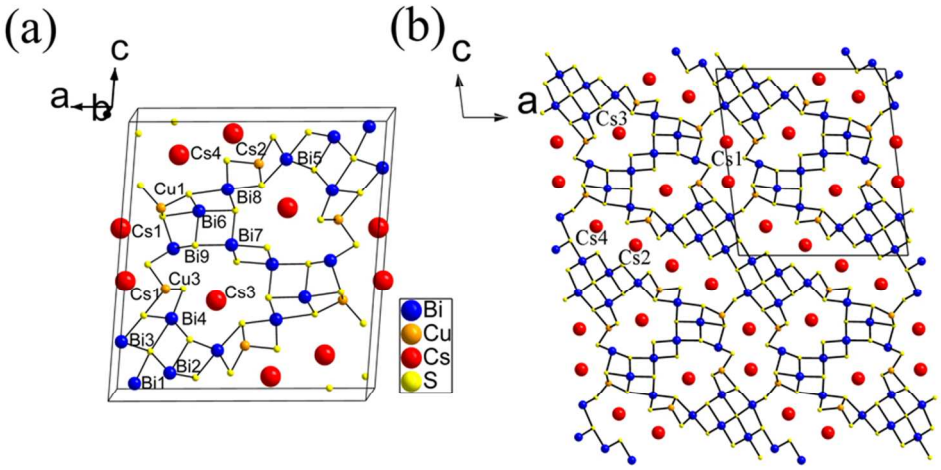

Figure 3. The unit cell (a) and the tunneled structure (b) of Cs4Cu3Bi9S17.

84x43mm (300 x 300 DPI)

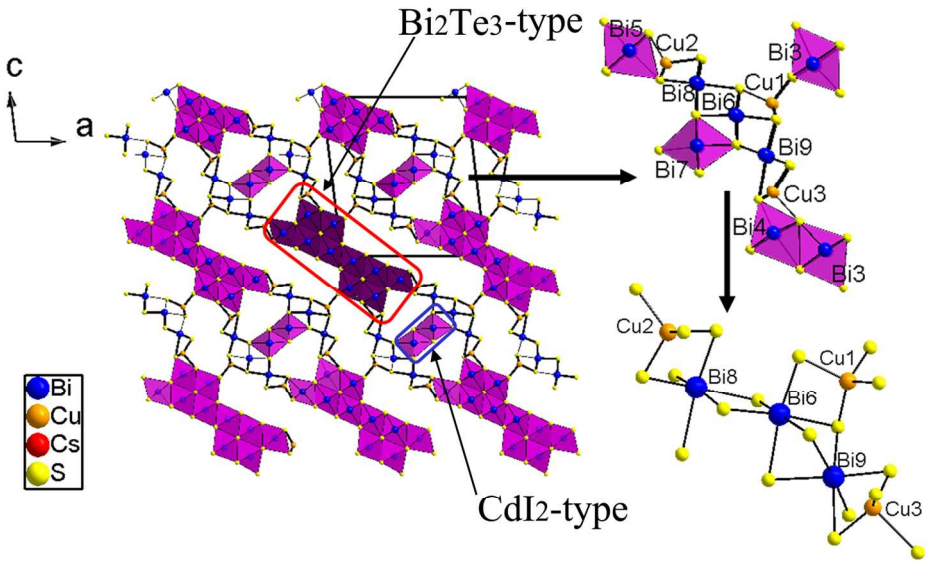

Figure 4. The framework of Cs4Cu3Bi9S17 which contains Bi2Te3- and CdI2-type blocks and three different sized tunnels in which cesium atoms reside; for clarity all Cs atoms were deleted. The frame on the right shows the details of the Bi- and Cu- polyhedra which connect the two different blocks together.

147x92mm (300 x 300 DPI)

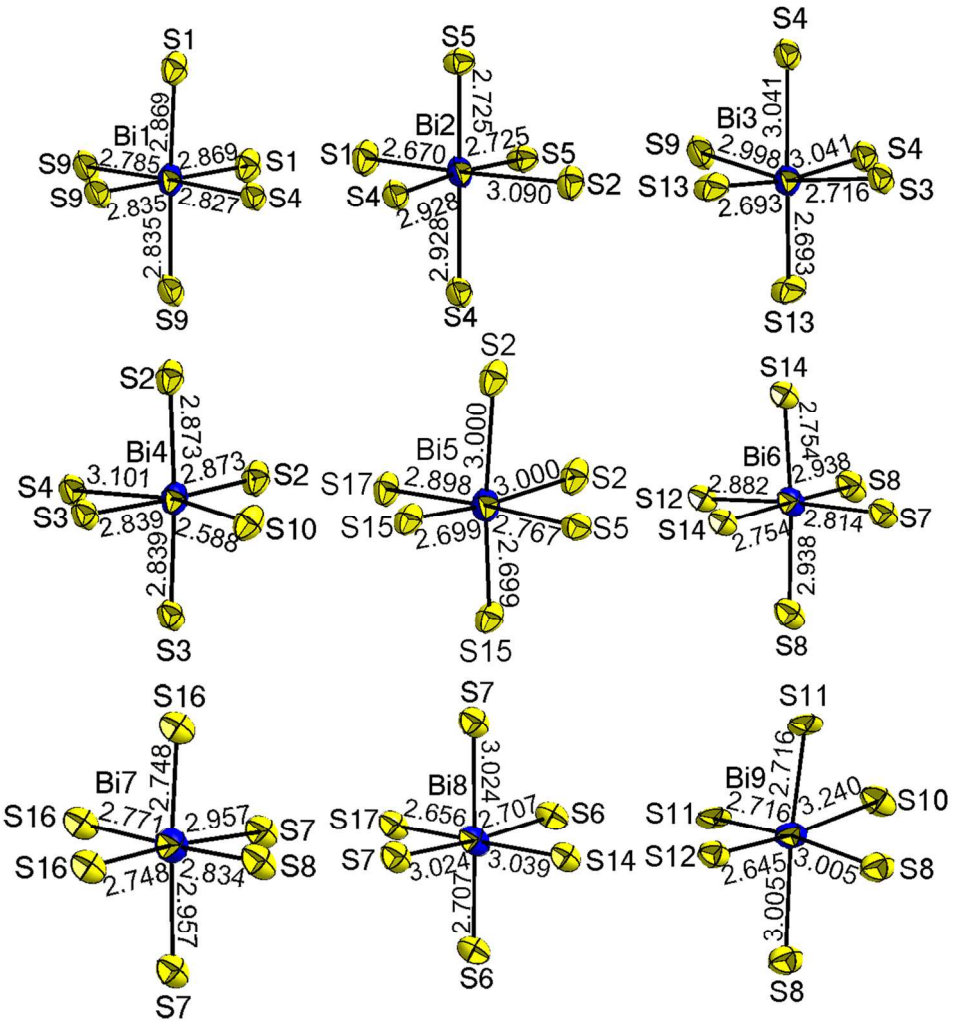

Figure 5. The coordination environments of Bi1 to Bi9.

150x155mm (300 x 300 DPI)

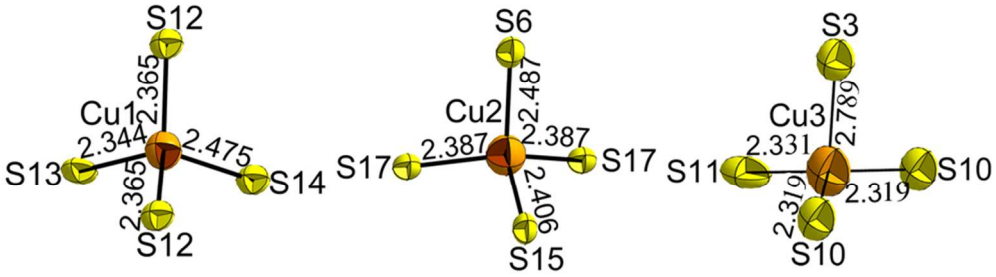

Figure 6. The coordination environments of Cu1, Cu2 and Cu3.

84x26mm (300 x 300 DPI)

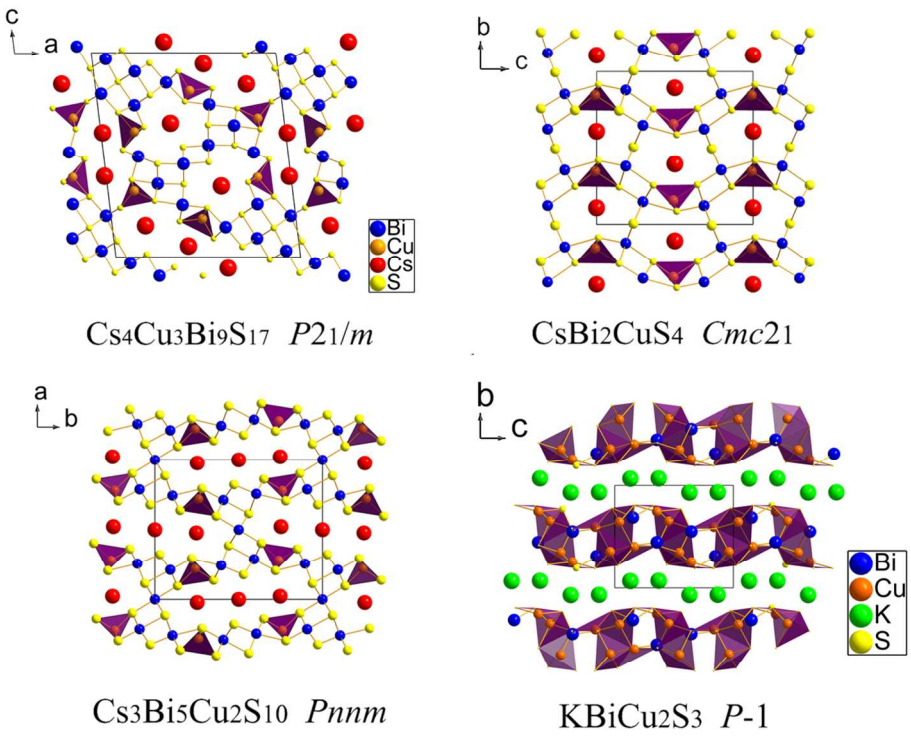

Figure 7. The structure comparison between Cs4Cu3Bi9S17 (this paper) and other reported A-Cu-Bi-S (A = alkali metal) compounds.

116x94mm (300 x 300 DPI)

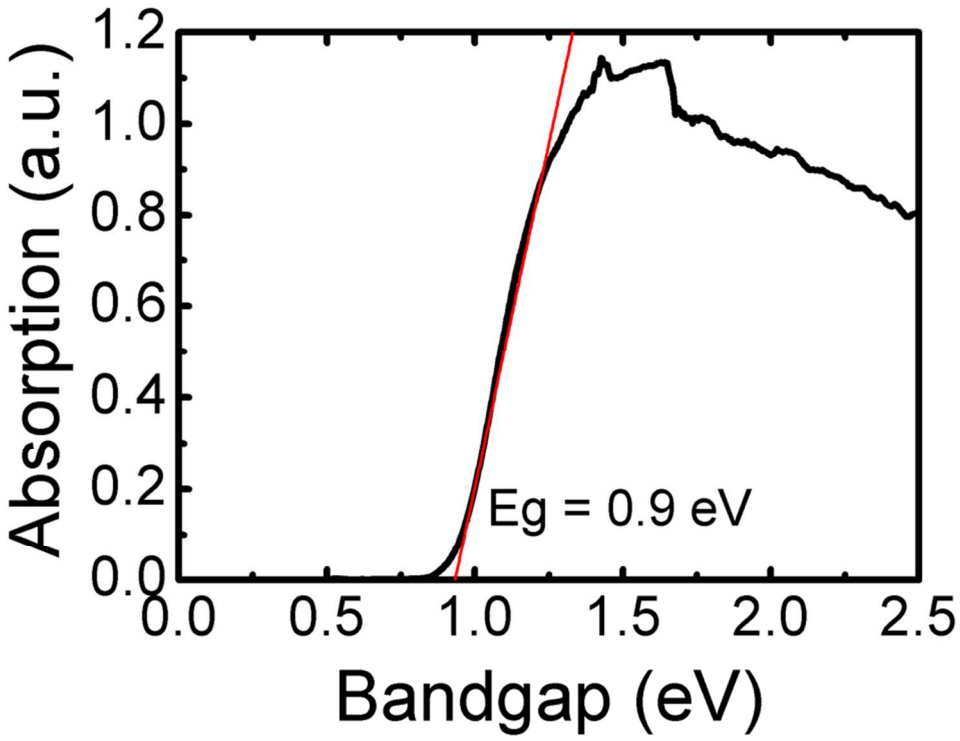

Figure 8. UV-vis spectrum of Cs4Cu3Bi9S17 which has a direct band gap of 0.9 eV.

84x65mm (300 x 300 DPI)

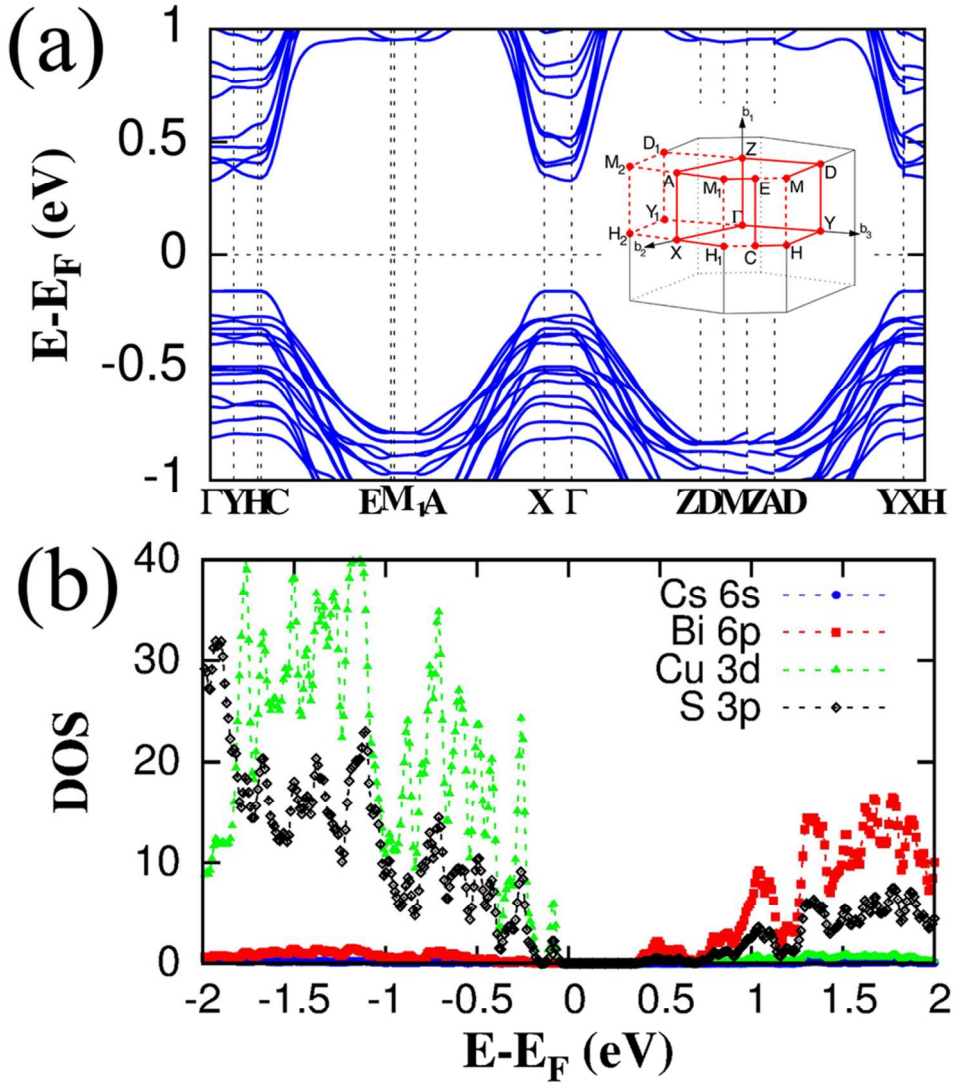

Figure 9. Band structure and corresponding Brillouin zone of Cs4Cu3Bi9S17; Total and partial density of states (DOS, eV/States) of Cs4Cu3Bi9S17.

84x95mm (300 x 300 DPI)

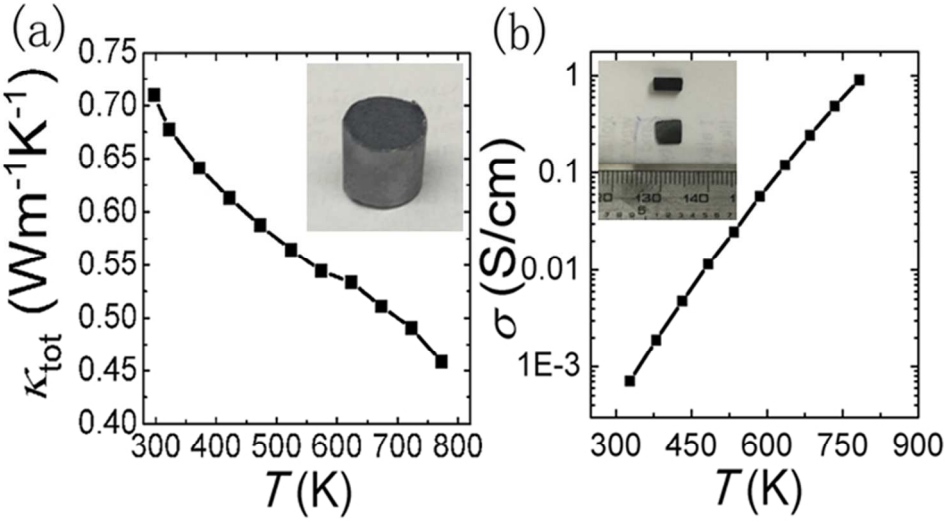

Figure 10. Thermal conductivity (a) and electrical conductivity (b) values as a function of temperature for Cs4Cu3Bi9S17; the inset shows the SPSed sample and the bar and cube used for measurements.

84x47mm (300 x 300 DPI)

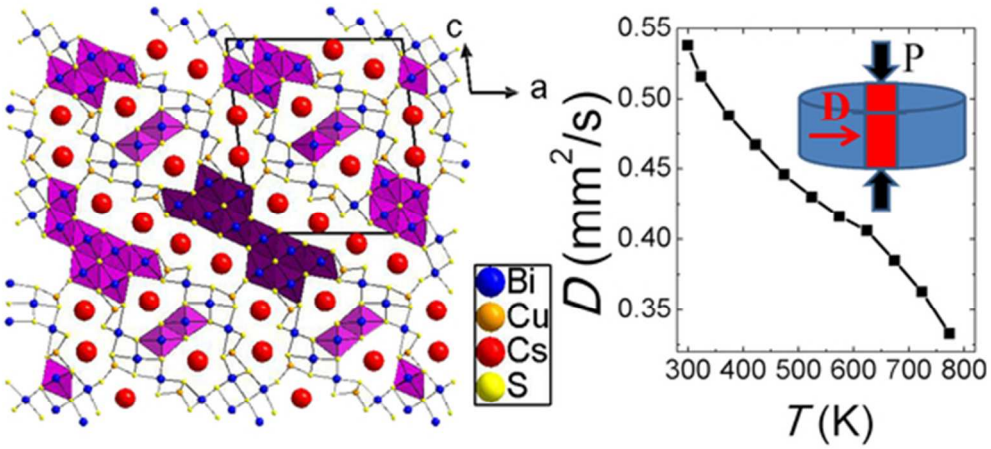

TOC

48x27mm (300 x 300 DPI)